Journal of Computational Science & Engineering 17 (2015) 569-575

Available at http://www.asocse.org ISSN 1710-4068

Influence of Relative Position between Vane and Volute Tongue on Hydraulic Performance of a Two-phase Flow Pump

Yingyu Ji[1]*, Fengrong Hu[2], Yuliang Zhang[1]

[1] College of Mechanical Engineering, Quzhou University, Quzhou, 412000, China

[2] College of Aeronautical Engineering Vocational and Technial, Jilin University of Chemical Technology, Jilin, 132000, China

Abstract: **To study the effect of the relative position between vane and volute tongue on external performance and interior flow field of a solid-liquid two-phase flow centrifugal pump, 3D numerical calculations of solid-liquid pump delivering two-phase flow are performed by using moving reference frame, RNG k-ε turbulence model, and mixture model. The pulsation character of external performance and variety character of interior flow field are achieved. Results show that some typical external parameters appear as periodic pulsation phenomena in the process of rotation, such as head, axis power, axial thrust, and radial force. Pulsation frequency is in proportion with rotation speed and vane numbers, and it actually embodies the unsteady flow characteristic of the pump. The volute tongue structure is the essential reason for the asymmetric flow field and the periodic pulsation in the pump.**

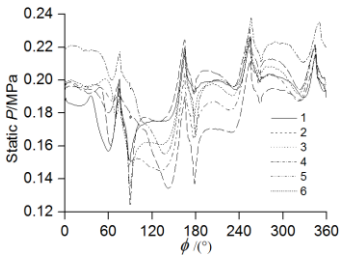

Keywords: Two-phase flow pump; Relative position; Numerical calculation; Pulsation characteristics

Received 22 December 2014, Revised 22 March 2015, Accepted 25 March 2015

* Corresponding Author: Yingyu Ji, turbomachinery@126.com

1. Introduction

Transport containing solid particles in two-phase flow pump is widely used in industrial and agricultural production, such as in the application of pulp pump to papermaking departments. The mud pump dredges the river in hydraulic departments. The sewage pump delivers the household waste in environmental protection departments. However, the flow of solid-liquid in two-phase is so complex that the existing design level of solid-liquid two-phase flow pump was much lower than the water pump. Theoretical research and design method on this aspect is still in the exploration and development stages. The mechanism of solid-liquid two-phase flow in the pump is still unknown. With the development of computational fluid dynamics and the rapid increase in computing power, we can quickly and effectively emulate and compute the flow pattern inside the pump. The development period of products could be shortened, and the test cost could be greatly reduced by using the numerical simulation technology.

A large number of studies in the country and abroad focus on the internal flow of a two-phase pump that transports particles by using the numerical simulation technology. However, these studies heavily concentrated on a relatively fixed position of the vane and volute tongue, which conducted the flowing numerical calculation [1-4]. The studies also considered multi-rotation directional calculation, but basically calculated for a single-phase flow [5-6]. Numerical calculation of two-phase flow and multi azimuth is still rare. To better reveal the internal flow regular pattern, a full range of numerical simulation studies should be carried out. At present, three methods can be used to achieve this aim: (1) moving mesh method [7-9]; (2) dynamic mesh method [10-11]; and (3) moving reference frame method [12-13]. These three methods have advantages and disadvantages. The first two can be used for unsteady flow calculation of arbitrary rotation bearing in theory, but because the flow is unsteady, performing a two-phase flow calculation will cost numerous computing resources and time. The dynamic mesh method is particularly prominent in this matter. The moving reference frame method could be used to calculate steady flow for different relative positions between the blade and the volute tongue. Steady flow was calculated many times, but because the flow is steady, the calculation time and resources were greatly reduced. Based on this, we adopted the third method to calculate the solid-liquid two-phase steady flow inside the pump model for different relative positions. The model pump considered has 4 blades of centrifugal impeller. The angle of adjacent blades is 90°. In this paper the marked position is regarded as the initial position, and rotating 15° is the next calculation position. Therefore, steady calculations are obtained 6 times in each computing rotation cycle.

2. Mathematical model

2.1. Governing equation

If using the C*v* represents the volume concentration of solid phase in two-phase flow, then in any one the volumes for Vm of two-phase flow, the volume of liquid phase is (1- C*v*) V*m* (1) Liquid phase momentum equation is as follows:

2015 © The American Computational Science Society. All rights reserved.

$$\frac{d\vec{u}}{dt} = \vec{F}_f - \frac{1}{\rho_f}\nabla p + \nu\nabla^2\vec{u} + \frac{\vec{F}_{sf}}{\rho_f(1-C_V)}$$

where $\vec{u}$ is the velocity vector of the liquid phase, $\vec{F}_f$ is the quality force vector of unit mass fluid, $\vec{F}_{sf}$ is the force vector of solid phase relative to liquid phase in the unit volume, and ρ_f is the liquid phase density.

(2) Solid phase momentum equation is

$$\left(1+C_\zeta\frac{\rho_f}{\rho_s}\right)\frac{d\vec{u}_s}{dt} - C_\zeta\frac{\rho_f}{\rho_s}\frac{d\vec{u}}{dt} = \vec{F}_s - \frac{1}{\rho_s}\nabla p + \frac{\vec{F}_{fs}}{\rho_s C_V}$$

Where $\vec{u}$ is the velocity vector of solid particles, $\vec{F}_s$ is the quality force vector of unit mass solid, $\vec{F}_{fs}$ is the force vector of liquid phase relative to solid phase in unit volume, C_ζ is a coefficient for spherical particles $C_\zeta = 0.5$, and ρ_s is the solid phase density.

(3) The continuity equation of solid phase, liquid phase respectively is as follows:

$$\frac{\partial(\rho_s C_V)}{\partial t} + \nabla\bullet(\rho_s C_V\vec{u}_s) = 0$$

$$\frac{\partial\left[\rho_f(1-C_V)\right]}{\partial t} + \nabla\bullet\left[\rho_f(1-C_V)\vec{u}_f\right] = 0$$

(4) The coupling equation of solid-liquid two-phase fluid is as follows: $\vec{F}_{sf} = -\vec{F}_{fs}$

2.2. Calculation model

The main design parameters of the centrifugal pump are as follows: the flow is 540m^3/h, the head is 25m, and the speed is 980r/min. The main geometric parameters are as follows: the impeller inlet diameter is D_1 = 230mm; the impeller outer diameter is D_2 = 450mm; the width at impeller outlet is 64*mm*; and the number of twisted blades is 4.

2.3. The Meshing

The mesh quality in computational domains directly determines the convergence accuracy of calculation. Therefore, the reasonable mesh should be generated based on the experiences and corresponding geometrical structure. In principle, the higher the grid number, the higher the calculation precision. However, a too-high grid number not only costs a great amount of computation time, but also does not show much effect on calculation accuracy. Therefore, from experience, obtaining a reasonable number of meshing is important to achieve computational efficiency and accuracy. In this computational domain, three calculation domains (the impeller rotating, the volute static, and impeller import extension areas) are obtained respectively to meshing by adopting the method of meshing sub-region. Grids are tetrahedral unstructured, and the total number of grids after dividing the calculation domain are 940000.

2.4. Boundary conditions

In this paper, the boundaries include the pump inlet, outlet, and the wall, and are described as follows:

(1) The inlet boundary conditions: to reduce the influence of inlet boundary conditions on the internal flow of the pump, the inlet is extended properly. In this paper, at the inlet of the computational domain, the velocity is selected as the boundary condition at the pump inlet. According to the conservation of mass and incompressible fluid properties, the axial velocity value at the inlet is given based on the regulated flow rate and the inlet pipeline size. It is assumed that the tangential and the radial velocities are zero. For precise calculation, the inlet of the turbulent kinetic energy k and turbulent dissipation rate ε of initial values can be determined by the following formula:

$$k = \frac{3}{2}(I\bar{u})^2 \qquad \varepsilon = C_\mu^{3/4}\frac{k^{3/2}}{l} \qquad I \approx 0.16\,\mathrm{Re}^{-1/8}$$

where l=0.07L, L is the characteristic length (in this paper, the value is the inlet diameter), I is turbulence intensity, $\mathrm{Re} = \bar{u}\cdot L/\nu$, and $\bar{u}$ is the average velocity of inlet. $C_\mu \approx 0.09$ is the empirical constant of the turbulence model.

(2) The outlet boundary conditions: in this paper, the flow at pump outlet is considered fully developed. Thus, the outflow is selected as the boundary condition of the pump outlet.

P_{out} is the velocity component, pout is the pressure, k_{out} is the turbulence kinetic energy, and ε_{out} is the turbulence dissipation rate. These are used as the second class boundary conditions, as follows:

$$\frac{\partial u_j|_{out}}{\partial\vec{n}} = 0,\ \frac{\partial p_{out}}{\partial\vec{n}} = 0,\ \frac{\partial k_{out}}{\partial\vec{n}} = 0,\ \frac{\partial\varepsilon_{out}}{\partial\vec{n}} = 0$$

$(j = 1,2,3)$

(3) The wall boundary conditions: because of the influence of fluid viscosity and the laws of physics, the no-slip and no-penetration boundary conditions are used on the wall. Near the model walls, the standard wall function is used in this paper.

2.5. Calculation method

In this paper, the RNG *k-ε* turbulent model is adopted to describe the turbulent flow in the pump, as proposed by YAKHOT in 1986[14]. The model is confined effectively to the flow inside the pump. The model can handle high strain rate and the great curvature of streamline flow. Based on the Euler–Euler method, mixture mixed model is adopted to describe the two-phase flow model [15]. It is assumed that the particles are homogeneous spherical particles with invariant physical properties. Solid particle diameter and solid phase concentration are 0.1 mm and 10% respectively, with the internal flow field calculated at the design point condition. The multiple reference frame used during simulation, the moving coordinate

2015 © The American Computational Science Society. All rights reserved.

system rotating with the synchronous impeller, and the static coordinate system fixed on the volute are established. In these two coordinates, all the speeds are converted into absolute speed, and the data exchange and coupling computation on the interface are accomplished. The control equations are discrete in space, and the discrete equation reflects the flow parameter in each calculation unit. To ensure the convergence of two-phase flow calculation, the momentum equation, the turbulent kinetic energy, and the turbulence dissipation rate adopt the first-order difference scheme. Pressure item adopts the standard format. The coupling between pressure and velocity is produced by using the SIMPLE algorithm. The convergence criteria of all calculated parameters are 0.001.

2.6. Calibration of initial calculation position

As shown in Figure 1, the marked blade location is at the first calculation position. Subsequently, each 15 ° is a calculated position along the rotation direction, and the calculation positions are marked by 1, 2, 3, 4, 5, and 6.

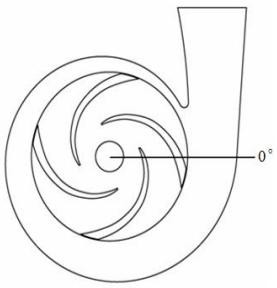

Figure 1. Diagram of initial calculation position

3. Result analysis

3.1. Pulse characteristics for each relative position

Pump internal flow presents pulsation phenomena at a design point [16～18]. It is shown as the external characteristic. Various physical quantities also present periodic pulsation. The physical quantity of pulse frequency in the model pump is 65 Hz. This frequency is proportional to the pump rotation speed and the number of blades. Because the pulsating frequency is relatively high, using ordinary measuring instruments cannot accurately measure the pulse value, and only the average value can be measured. Thus, the flow calculation in a relative position provides the external characteristic, but cannot accurately predict the true value. We need to get the average value by the multi-phase calculation to fully reflect the unsteady flow characteristics. The head, efficiency, shaft power, axial force, radial force, and direction are selected for characterization. The pulsating characteristics inside the pump are obtained after calculation and are presented in Figure 2. For different relative positions between the volute tongue and the rotating blade, the maximum head fluctuation is up to 1.7 m, whereas the minimum of the heads is only 18.76 m. Consequently, the relative error is 9%. Relative to the minimum obtained in the process of pulsation, pulsation amplitude is still great. When the blade is nearest to the volute tongue, the pulsation head of the pump is minimal. When the two relative positions are farthest, the pulsation head is maximum. The maximum difference of the shaft power is up to 3.26 kw, and the maximum difference of the efficiency is up to 6%. The variation characteristics are consistent with that of the head pulsation in a changing rule.

For a centrifugal pump, the axial force is very important for the design of the balancing device [19]. Excessive axial force would pull the rotor for moving along the axial direction. The pump parts would be damaged and would not be able to work when in contact with each other. At relative position 6, i.e., when the blade is a little behind the volute tongue, the axial force shows a maximum value. With a spiral pressurized water chamber of the pump, the radial forces generated during operation act on the impeller [20], the radial forces result in periodic alternating stress on the shaft, and the deflection of a certain direction ensues. In the calculations, the spiral volute has no radial force in theory. However, because the change of relative position leads to periodic change in the radial force, the change will cause the pump's vibration. Thus, the base fixed should be considered. As calculated in this paper, the resultant force of radial force with horizontal angle is about 85 ° in the vertical direction.

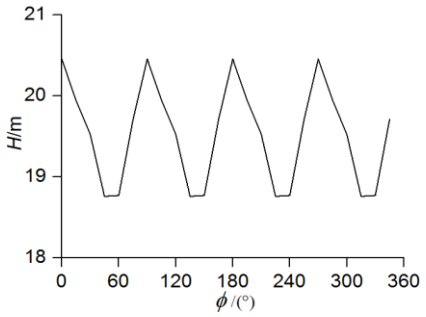

(a) head

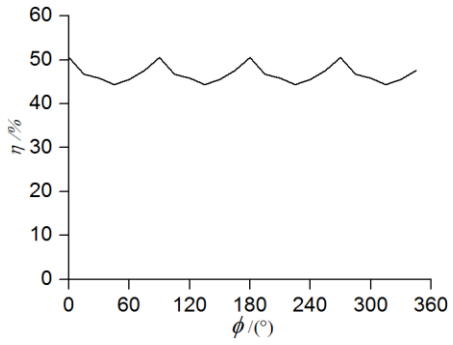

(b) efficiency

2015 © The American Computational Science Society. All rights reserved.

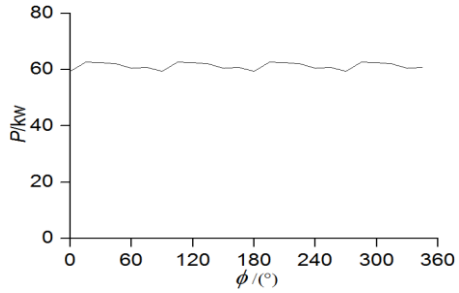

(c) shaft power

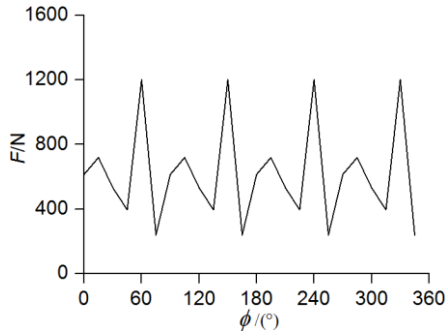

(d) axial force

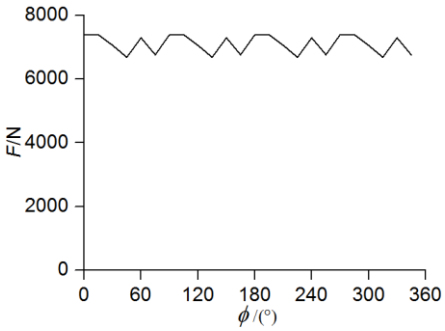

(e) radial force

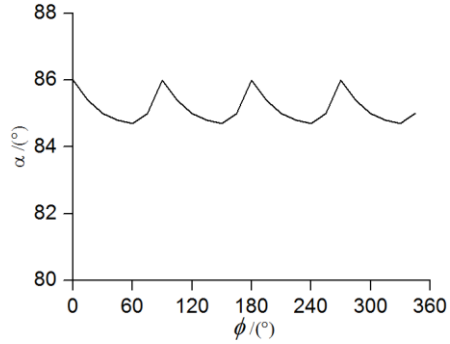

(f) change of radial force direction

Figure 2. Pulsating curve of various physical quantities

3.2. Distribution characteristics of physical parameters

The distributions of the static pressure, velocity, and solid volume fraction along the circumference on the middle section of impeller are selected as the classical parameters for the study of variable characteristics. The results are shown in Figure 3. The distributions of static pressure and solid volume fraction at different relative positions appear markedly changed, but the entire evolution trend at each position is similar. Thus, the distribution law of static pressure and solid particles are also dynamic in the process of impeller rotation. However, we can see that the distribution laws of velocity at different relative positions are approximately similar. These results could be attributed to the fact that the flow rate determines the magnitude of velocity, and the circumference speed is not variable under the condition of a constant rotational speed.

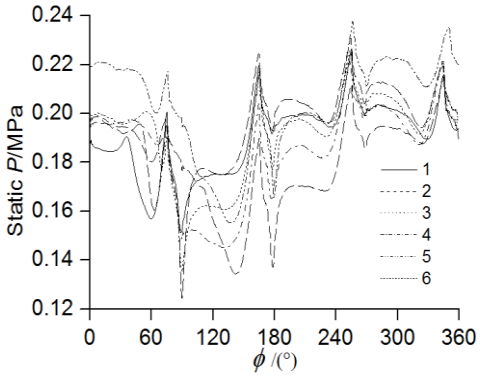

(a) static pressure

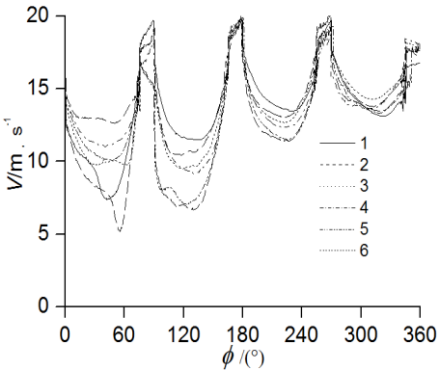

(b) velocity

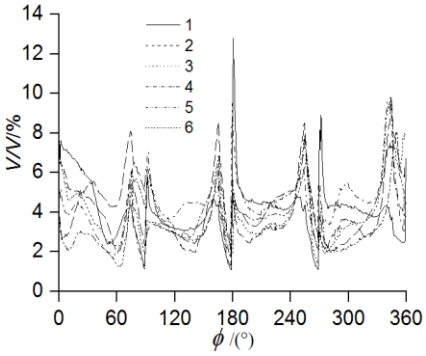

(c) solid volume fraction

Figure 3. Distribution characteristics of physical parameters

2015 © The American Computational Science Society. All rights reserved.

3.3. Internal flow field at each relative position

(1) Static pressure

Figure 4 shows the static pressure change on the middle section of the impeller. The static pressure increases with the increase of radius at any relative position. Consequently, the obvious zonal distribution is clearly displayed. However, for the blades' work, the pressure on the surface of blade is significantly higher than the pressure on the back at the same radius. The pressure difference on both sides makes the fluid in each flow channel of the impeller work. The pressure and potential energies are produced. The flow area of the channel is seriously decreased because of the blocking at the blade inlet. At that time, the rotating blades are not able to provide the required energy, thereby directly causing the acceleration of flow velocity and the reduction of pressure while flowing around the blade inlet. The minimum area of static pressure occurs at the blade back, which is located slightly after the inlet. The corresponding changes mainly occur in the impeller passage near the volute tongue for each relative position. In this channel, the internal flow is very complex, and the change is very serious. Relative to the channel near the volute tongue, the flow is more regular away from the volute tongue. The pressure difference is maximum at both sides of the blade near the volute tongue. At a distance away from the volute tongue, the pressure difference is relatively small. In the process of blade rotation, i.e., the calibrated blade rotates from position 1 to the volute tongue, the minimum static pressure area from slightly behind the inlet gradually transfers to the inlet. This circumstance is the result of the interaction between impeller and volute. The static pressure is largest outside the volute wall, whereas the changes are very dramatic near the volute wall. Meanwhile, the distribution of static pressure is more regular in the diffusion tube.

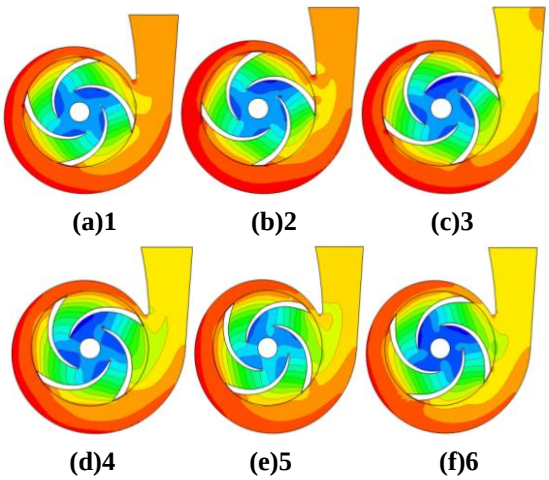

Figure 4. Static pressure change on the middle section

(2) Total pressure on the middle section of impeller

Figure 5 shows the total pressure change on the middle section of the impeller. Although the impeller passage gradually expands, the relative flow velocity decreases. The increase of the radius leads to the increase of peripheral speed. Thus, the kinetic energy also increases rapidly, and this result is nearly in agreement with the static pressure distribution. The total pressure at any position increases with increasing radius. Meanwhile, the total pressure on the working surface of the blade is obviously higher than that on the back at the same radius position. This finding can be attributed to the following: the kinetic energy, which is represented by velocity, does not change in the process of rotation. Thus, the distribution regularity of the total pressure is nearly in agreement with the static pressure distribution.

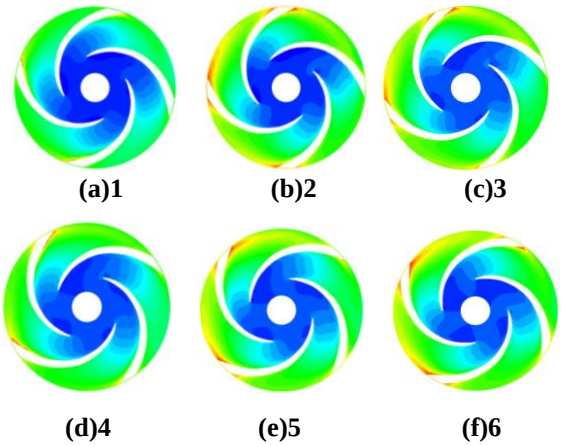

Figure 5. Total pressure change on the middle section

(3) Total pressure around volute tongue

Figure 6 shows the total pressure change around the volute tongue on the middle section of the impeller. When the blade rotates close to the volute tongue, the obvious trend is that the total pressure gradient clearly increases near the volute tongue.

When the blade passes the volute tongue, the total pressure gradient begins to decrease gradually. Thus, the maximum total pressure gradient caused by hydraulic loss is most serious at the location nearest to the tongue, which leads to the decline of the head, and is identical with the pulsation characteristics of the calculated head.

When the process of blade rotation sweeps across the volute tongue, the fluid from flow channels is divided into two parts; one part enters the volute, and another part directly flows into the volute throat. In the entire process of rotation through the volute tongue, the fluid volume running to the throat in this flow channel decreases gradually. Clearly, the rising pressure could be obtained by decreasing the flow velocity in the diffuser.

2015 © The American Computational Science Society. All rights reserved.

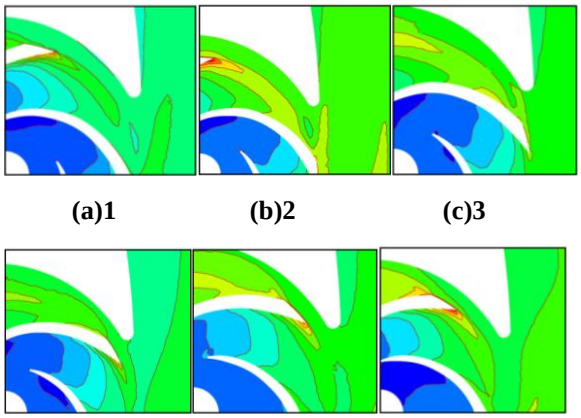

Figure 6. The total pressure change around the volute tongue on the middle section

(4) The second section streamline of volute

Figure 7 shows the vortex structure change of the volute in the second section. Because of the change of the relative position of the blade and the volute tongue, obvious changes have been taking place in the secondary flow structure in the second section of volute. The general evolution rule is that in any position before and after the blade rotating sweeps across the volute tongue, the secondary flow structure appears bigger and more vortex structured. Moreover, the vortex intensity is greater. These new vortex structures will lead to more hydraulic loss in the volute, after which the pump head drops. The appearance of this flow structure obviously relates directly to the external characteristic pulsation head drop and the total pressure gradient change near the volute tongue.

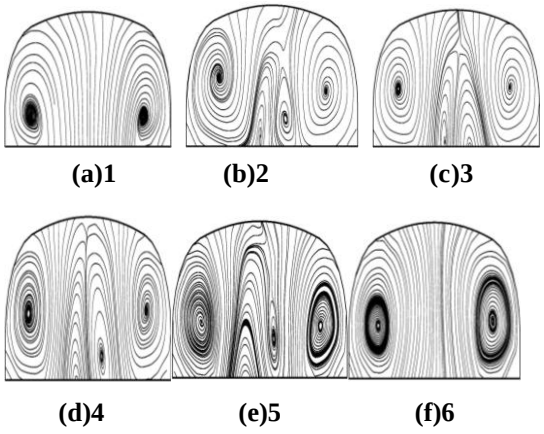

Figure 7. Vortex structure change of the volute in the second section

(5) The eighth section streamline of volute

Figure 8 shows the vortex structure change of volute in the eighth section. The shape and area of the throat greatly affect the external characteristics of the pump. Because the eighth section is close to the throat position, the analysis of the characteristics for the eighth section could directly represent the throat characteristics. In this paper, the width at volute inlet is relatively large to absorb the energy from the front and back chambers. This design directly results in two symmetrical vortices appearing in either side of second and eighth sections. From the changes of flow vortex in the secondary and eighth sections, we determine that the flow is close to stable at this time. The velocity magnitude of high-speed fluid from the impeller channels dramatically decreases so that its pressure energy is augmented after the flowing pump volute.

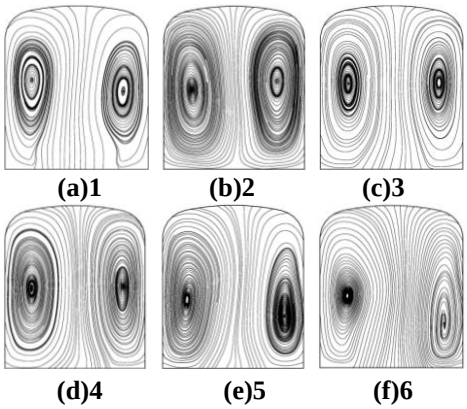

Figure 8. Vortex structure change of volute in the eighth section

4. Conclusions

(1) The head, shaft power, axial force, and radial force of the pump model show the characteristics of periodic pulsation during rotation, which is consistent with the fluctuating characteristics of the pump's unsteady flow. (2) The asymmetric characteristics of the volute caused by the tongue structure are the fundamental reasons for uniform flow fields and periodic pulsation.

Acknowledgements

The work was support by the Zhejiang Provincial Natural Science Foundation of China (No.LY14E090011).

References:

[1] J.F. Zhang, S.Q. Yuan, Y.D. Fu, Journal of Mechanical Engineering, 7 (2009) 131-137.
[2] W. Jiang, G.J. Li, X.S. Zhang, Journal of Drainage and Irrigation Machinery Engineering, 5 (2013) 205-209.
[3] Y.L. Zhang, Y. Li, B.L. Cui, Journal of Mechanical Engineering, 14 (2012) 169-176
[4] G. Pavesi, G. Cavazzini, G. Ardizzon, International Journal of Heat and Fluid Flow, 29 (2008) 1527-1540.
[5] X.Y. Wang, C.X. Wang, Chinese Quarterly of Mechanics, 4 (2007) 619-623.
[6] Y. Wang, C. Dai, Transactions of the Chinese Society for Agricultural Machinery, 11 (2009) 89-93.
[7] B.J. Zhao, S.Q. Yuan, H.L. Chen, Transactions of

2015 © The American Computational Science Society. All rights reserved.

the Chinese Society for Agricultural Machinery, 6 (2009) 115-119.
[8] S. Huang, Q.J. Deng, H.J. Wang, Fluid Machinery, 3 (2009) 24-27.
[9] S.L. Wang, L.Tan, Y.C. Wang, Journal of Vibration and Shock, 22 (2013) 168-173.
[10] F. Jiang, W.P. Chen, Y.J. Wang, Fluid Machinery, 7 (2007) 20-24.
[11] J. Zhang, X.Y. Qi, Y.H. Hou, Transactions of the Chinese Society for Agricultural Machinery, 1 (2009) 64-68.
[12] J.F. Zhang, W.J. Wang, Y.J. Fang, Journal of Vibration and Shock, 23 (2014) 37-41.
[13] S.Q. Yuan, L.T. Ye, J.F. Zhang, Journal of Drainage and Irrigation Machinery Engineering, 4 (2012) 373-378.
[14] S.J. Zhang, X.H. Li, B.L. Zhu, Journal of Mechanical Engineering, 4 (2009) 238-242.
[15] B.J. Zhao, S.Q. Yuan, H.L. Liu, Simulation of solid-liquid two-phase turbulent flow in double-channel pump based on Mixture model, 1 (2008) 7-12.
[16] Y.C. Wang, L. Tan, S.L. Cao, Journal of Mechanical Engineering, 10 (2014) 163-169.
[17] R. Spence, J. Amaral-Teixeira, Computers & Fluids, 38 (2009) 1243-1257.
[18] Q.R. Si, S.Q. Yuan, J.P. Yuan, Fluid Machinery, 8 (2012) 22-26.
[19] W.D. Shi, Q.F. Li, W.G. Lu, Transactions of the Chinese Society for Agricultural Machinery, 1 (2009) 60-63.
[20] W.Y. Zhao, L. Zhang, J. Luo, Drainage and Irrigation Machinery, 27 (2009) 205-209.

2015 © The American Computational Science Society. All rights reserved.